PROC. INST. ACOUSTICS VOL 6 PT 3 1984

Envelope Statistics of Multipath Propagation in the Ocean

Peter N. Mikhalevsky
Department of Ocean Engineering (5-204)
Massachusetts Institute of Technology
Cambridge, Mass 02139

Abstract and Introduction

In many practical problems involving sound propagation in the ocean the received signal pressure can be modeled as a sum over many independent paths connecting the source to the receiver and this is commonly referred to as multipath propagation. It is also commonly understood that multipath generally degrades receiver performance as it causes signal energy to be spread in time due to differing path lengths and in frequency due to path to path differential doppler, or ocean dynamic induced sound speed fluctuations affecting each path differently. This paper discusses the envelope statistics of narrowband signals in three multipath regimes and the consequences for receiver performance. The three regimes are referred to as unsaturated, partially saturated, or fully saturated, as delineated by the degree of path to path phase stability. Additionally, data taken in the Arctic Ocean are shown to be in the unsaturated regime attesting to the Arctic sound channel's remarkable temporal stability at low frequencies. It should also be noted that these data were the first such calibrated coherent source data taken in the Arctic Ocean. The source is an electrically operated hydraulic piston that modulates a flexural disc radiator.

I. The Multipath Environment

Sound propagating in the ocean at low frequencies, less than several hundred Hz over ranges >100 km arrive via many independent paths at the receiver. In general the number of independent paths can be determined from wave theory as the number of propagating modes in the acoustic duct. An upper bound on this number for an isovelocity profile over a hard bottom is approximately twice the duct thickness divided by the acoustic wavelength. For the data from the Arctic presented later in this paper the number of propagating modes was calculated to be approximately ten. When the number of paths is greater than 4 as is true for most practical ocean acoustic cases and all of the paths are approximately equally energetic (e.g. <6db variation) then the statistical properties of the received multipath field approach limiting forms. If we consider narrowband signals the important statistical properties that influence receiver detection performance include the statistics of the amplitude and phase of the received signal envelope. The quadrature components of the envelope of a narrowband multipath process are given by [Ref. 1,2],

$$X = \sum_{n=1}^{N} (r_n \cos\theta_n + N_x^{(n)}) \,, \qquad Y = \sum_{n=1}^{N} (r_n \sin\theta_n + N_y^{(n)}) \,, \tag{1}$$

where N is the number of independent paths between source and receiver, r_n is the single path amplitude at the receiver (assumed to be approximately equal for all paths), θ_n is the phase of the nth path, and $N_x^{(n)}$ and $N_y^{(n)}$ are zero mean uncorrelated Gaussian additive noise for the nth path. The envelope amplitude ρ, and its phase ϕ, are given by the square root of the sum of the squares of X and Y, and the Arg (Y/X), respectively. We characterize θ_n as a Gaussian random variable as a consequence of the assumption that the perturbations experienced by a path are the cumulative effect of many independent actions along the entire path. This implies that the total unperturbed path length is much greater than the correlation length of the ocean dynamic processes that cause the sound-speed fluctuations along the path. I define the mean of θ_n as $\mu_\theta^{(n)}$ and the variance as σ_θ^2. As indicated by the notation I assume that the mean may vary from path-to-path but that the variance is the same. The mean phase of any multipath will be a function of the unperturbed path length. The variance will be a function of the perturbations experienced along the entire path. As long as the differences in path lengths are much less than the mean path length then homoscedasticity is reasonable. This conclusion implies that the perturbations experienced on each path are similar and therefore applies to paths undergoing the same kind of propagation, e.g., RSR paths, BB paths, or SOFAR paths, but not mixtures of such paths. It is the variance of θ_n, σ_θ^2 that dominates the character of the envelope statistics and delineates the three mulipath regimes described above.

Fully saturated propagation obtains when $\sigma_\theta \to \infty$ which in actual fact implies $\sigma_\theta \gtrsim \pi/2$ (which closely approximates the standard deviation of uniformly distributed θ_n between 0 and 2π). In this regime the probability density function (pdf) of ρ is Rayleigh, and the pdf of ϕ, the multipath phase is uniformly distributed between 0 and 2π. In the limit as $\sigma_\theta \to 0$ the propagation approaches the unsaturated regime. In the absence of scattering randomness, and in the presence of additive Gaussian noise the pdf of the amplitude is Rician. When $0 < \sigma_\theta < \pi/2$ the propagation is in the partially saturated regime. In this case it can be shown that the pdf for ρ is given by [3],

$$p_\rho(\rho) = \frac{\rho}{2\pi\,\sigma_X\sigma_Y\,(1-\rho_{xy}^2)^{1/2}} \exp\left[\frac{-1}{2(1-\rho_{xy}^2)}\left(\frac{\rho^2+2\mu_X^2}{2\sigma_X^2} - \frac{2\rho_{xy}\mu_X\mu_Y}{\sigma_X\sigma_Y} + \frac{\rho^2+2\mu_Y^2}{\sigma_Y^2}\right)\right]$$

$$\times \int_0^{2\pi} d\phi \exp\left[\frac{-1}{2(1-\rho_{xy}^2)}\left(a\cos(2\phi) + b\sin(2\phi) + c\cos\phi + d\sin\phi\right)\right] \qquad \ldots(2)$$

where

$$a = \rho^2\left(\frac{1}{2\sigma_X^2} - \frac{1}{2\sigma_Y^2}\right)$$

$$b = -\rho^2\frac{\rho_{xy}}{\sigma_X\sigma_Y}$$

$$c = \rho\left(\frac{2\rho_{xy}\mu_Y}{\sigma_X\sigma_Y} - \frac{2\mu_X}{\sigma_X^2}\right)$$

$$d = \rho\left(\frac{2\rho_{xy}\mu_X}{\sigma_X\sigma_Y} - \frac{2\mu_Y}{\sigma_Y^2}\right)$$

and,

$$\mu_X = \sum_{n=1}^{N} r_n \cos(\mu_\theta^{(n)}) \exp(-\tfrac{1}{2}\sigma_\theta^2)$$

$$\mu_Y = \sum_{n=1}^{N} r_n \sin(\mu_\theta^{(n)}) \exp(-\tfrac{1}{2}\sigma_\theta^2)$$

$$\sigma_X^2 = \sum_{n=1}^{N} \frac{r_n^2}{2}\left[1 - \exp(-\sigma_\theta^2) + A\cos(2\mu_\theta^{(n)})\right] + \sigma_N^2$$

$$\sigma_Y^2 = \sum_{n=1}^{N} \frac{r_n^2}{2}\left[1 - \exp(-\sigma_\theta^2) - A\cos(2\mu_\theta^{(n)})\right] + \sigma_N^2$$

$$\rho_{XY} = \frac{-\exp(-\sigma_\theta^2)\sum_{n=1}^{N} r_n^2 \sin(2\mu_\theta^{(n)})}{\left\{\sum_{n=1}^{N} r_n^2 - \exp(-2\sigma_\theta^2)\left[\sum_{n=1}^{N} r_n^2 \cos(2\mu_\theta^{(n)})\right]^2\right\}^{1/2}}$$

$$A = \exp(-2\sigma_\theta^2) - \exp(-\sigma_\theta^2)$$

Equ.(2) has been plotted for several values of σ_θ in Fig. 1. N was chosen to be 10, the $r_n = 1$ for all n, and an arbitrary set of $\mu_\theta^{(n)}$ [3] was chosen. Although N = 10 in this example (for computation of the moments given above), Equ. (2) is the limiting form of the pdf as $N \to \infty$. σ_N^2 was chosen such that the SNR = 15 db as indicated in Fig. 1. From Fig. 1 we can see that as $\sigma_\theta \to 0$ and as $\sigma_\theta \to \infty$ the unsaturated and fully saturated results are obtained respectively. As indicated above the Rician density obtains in the absence of scattering randomness which has not been formally included in the foregoing analysis. To the extent that scattering randomness causes fluctuations in the phase that contribute to the total phase variance σ_θ^2, it is included. Also implicitly included in the analysis is the effect of mean scattering loss on each path under the assumption that each path experiences the same loss. It is the fluctuations of the single path amplitude r_n that has been neglected (e.g. $d/dt\,[r_n] \ll 1$). For the case of large N, as assumed here, and as σ_θ becomes large ($\geq \pi/2$) it has been shown that the random phases in the multipath sum dominate the statistics [1]. When $\sigma_\theta \to 0$ neglect of random variations in r_n must be suspect and may be comparable in effect on the envelope statistics as that caused by the phase fluctuations. For data analysed in the Arctic [4] where $\sigma_\theta \approx 0$ neglect of single path amplitude fluctuations is shown to be justified.

II. Data Analysis

Continuous wave (CW) acoustic signals were propagated via an ice-covered path over a range of approximately 300 km between two ice camps as part of the TRISTEN/FRAM II East Arctic experiment conducted in April and May of 1980 [5,6]. Data at 15, 20, and 30Hz were analyzed. The data were recorded on a 24 channel 800 by 800 m L-shaped horizontal array. The array data were beamformed using a standard delay and sum technique. After beamforming each tone was quadrature demodulated, low pass filtered, decimated and low pass filtered again. The result is a 128 mHz passband centered on the demodulated tone. The envelope and phase of these data were formed from the quadrature components. In Figs. 2 and 3 are plotted the log of the amplitude of the envelope and the phase of the envelope, respectively, for a 30 Hz tone. Note the exceptional stability in amplitude and phase. The mean phase varies by <0.03 cycles in 30 minutes. A total of

five hours of data were analyzed. All these data exhibit similar stability.

We can represent the received narrowband filtered demodulated CW tone using a polar plot as shown in Fig. 4. Note that the signal vector is composed of many single path vectors. Any fluctuations in the total vector will depend upon the fluctuations in the single path phases and/or amplitudes, and the noise. In general, if we filter the data in a narrow enough band, then the contribution of the noise to the fluctuations of the envelope will be negligible compared with the fluctuation of the single path vectors. For these data from the Arctic, filtering in narrower and narrower bands to the limit imposed by the length of the time series always reduced the envelope fluctuations. This implies that not only is $\sigma_\theta \approx 0$ but that the single path amplitudes are constant as well. To test this hypothesis we apply the Rician model for the unsaturated regime. Refering to Fig. 4 we write the Rician pdf for the envelope amplitude ρ [7],

$$p_\rho(\rho) = (\rho_s/\sigma_N^2) \exp\left[-(\rho^2+\rho_s^2)/2\sigma_N^2\right] I_o(\rho\rho_s/\sigma_N^2) \qquad (3)$$

where ρ_s is the amplitude of the constant signal vector, σ_N^2 is the noise power in the band, and $I_o(z)$ is Bessel's function of the first kind of zero order. Equ. (3) can be obtained directly from Equ. (2) by setting $\sigma_\theta = 0$ and noting that $\rho_s^2 = \mu_x^2 + \mu_y^2$.

For all these data σ_N^2 is measured directly, just prior to or after the tone was in the water. It is verified that the noise is in fact Gaussian using a chi-square test at a .05 level of significance [4]. From plots of the log amplitude (Fig. 2) ρ_s is estimated by eye. With these two values Equ. (3) is plotted with the histogram of the data and the chi-square test is applied. For all the data analyzed the chi-square test was passed at the .05 level of significance [4]. An example of a data histogram and Equ. (3) for the envelope amplitude is shown in Fig. 5. Thus for these data the model is valid, but more importantly the exceptional temporal stability of the Arctic channel is demonstrated. It is important to note, however, that the transmission path was between two ice camps with negligible relative drift so these results apply to terminals essentially fixed with respect to the water column motion.

III. Detecting the Signal

The optimal receiver structure for detecting CW tones in the multipath environment can be derived by constructing the likelihood ratio for optimal detection under the classical binary hypothesis test [8]. The two hypotheses can be denoted H_o, or the null hypothesis that no signal is present, and H_1, the hypothesis that the signal is present. Assuming the noise is Gaussian in quadrature and therefore Rayleigh in amplitude the probability of observing amplitude $\tilde{\rho}$ under the null hypothesis H_o is

$$p_\rho(\tilde{\rho}\,|\,H_o) = (\tilde{\rho}/\sigma_N^2) \exp\left[-(\tilde{\rho}^2/2\sigma_N^2)\right] \qquad (4)$$

where σ_N^2 is the noise variance. The probability of observing amplitude $\tilde{\rho}$ under the hypothesis that the signal is present H_1 is

$$p_\rho(\tilde{\rho}\,|\,H_1) = \text{Equ. (2)}\,\Big|_{\rho=\tilde{\rho}} \qquad (5)$$

Given Equs. (4) and (5) construction of the likelihood ratio $\Lambda(\tilde{\rho})$ is straightforward

$$\Lambda(\tilde{\rho}) = p_\rho(\tilde{\rho}\,|\,H_1) \big/ p_\rho(\tilde{\rho}\,|\,H_0) \tag{6}$$

and the corresponding decision rule is to decide H_1 iff $\Lambda(\tilde{\rho}) > \eta$, otherwise H_0.

Following Ref. 9 after applying Equs. (4) and (5) in Equ. (6) we note that the function Λ is a positive, monotonically increasing function of $\tilde{\rho}$, and thus a unique inverse function Λ^{-1} exists. Therefore we decide H_1 iff $\tilde{\rho} > \lambda = \Lambda^{-1}(\eta)$. This implies that noncoherent envelope detection is optimal to detect the partially saturated signal. The probability of detection P_D and the probability of false alarm P_F can be written as

$$P_D = \int_\lambda^\infty p_\rho(\tilde{\rho}\,|\,H_1)\, d\tilde{\rho} \tag{7}$$

and

$$P_F = \int_\lambda^\infty p_\rho(\tilde{\rho}\,|\,H_0)\, d\tilde{\rho} \tag{8}$$

Equs. (7) and (8) define the receiver operating characteristics (ROC) of the optimal receiver for the detection of the signal. Furthermore, in the limit as $\sigma_\theta \to 0$ and $\sigma_\theta \to \infty$ the ROC for Rician and Rayleigh fading signals in Gaussian noise are obtained, respectively.

In Fig. 6 the probability of detection given by Equ. (7) is plotted versus SNR at a fixed false alarm rate of 10^{-6}. For a probability of detection of 0.9, 5 dB more signal-to-noise is required to obtain the 10^{-6} false alarm rate with $\sigma_\theta = \pi/4$ as compared to the constant Rician signal. With $\sigma_\theta = \pi/2$ the limiting result ($\sigma_\theta = \infty$) is closely approximated and to obtain the same detection probability at $P_F = 10^{-6}$ will require almost 15 dB more signal-to-noise. It is apparent that increasing saturation (σ_θ increasing from 0 to ∞) quickly degrades performance.

IV. Discussion and Conclusions

A statistical model for multipath acoustic propagation of narrowband tones in the ocean has been presented. For the sake of brevity only the envelope amplitude statistics have been discussed. Comparison with data in the fully saturated regime [2] (not presented here), and in the unsaturated regime is favorable. Remaining issues include data comparison in the partially saturated regime and most important, identifying and quantifying the relevant ocean physics or ocean dynamic processes upon which σ_θ depends, particularly at low frequencies.

References

[1] I. Dyer, J.Acoust.Soc.Am. 48, 337-345 (1970).

[2] P.N. Mikhalevsky, J.Acoust.Soc.Am. 66, 751-762 (1979).

[3] P.N. Mikhalevsky, J.Acoust.Soc.Am. 72, 151-158 (1982).

[4] P.N. Mikhalevsky, J.Acoust.Soc.Am. 70, 1717-1722 (1981).

[5] F. DiNapoli, et al., "TRISTEN/FRAM II Cruise Report," Naval Underwater Systems Center Technical Document 6457 (May 1981).

[6] A.B. Baggeroer and I. Dyer, "FRAM II in the Eastern Arctic," EOS, Trans.Am. Geophys. Union April 6, 1982.

[7] S.O. Rice, Bell Syst.Tech.J. 23, 282-332 (1944); 24, 46-156 (1945).

[8] H.L. Van Trees, Detection, Estimation, and Modulation Theory (Wiley, New York, 1968), Part I.

[9] J.K. Jao and M. Elbaum, Proc. IEEE 66, 781-789 (1978).

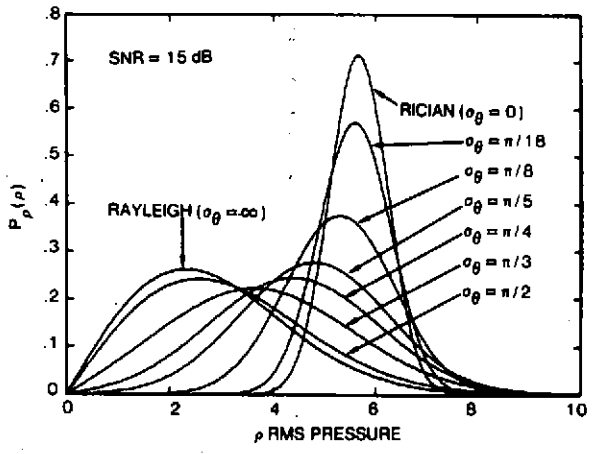

Fig. 1. The pdf of the envelope amplitude ρ, Equ. (2), with additive Gaussian noise such that the SNR = 15 , plotted for various values of σ_θ.

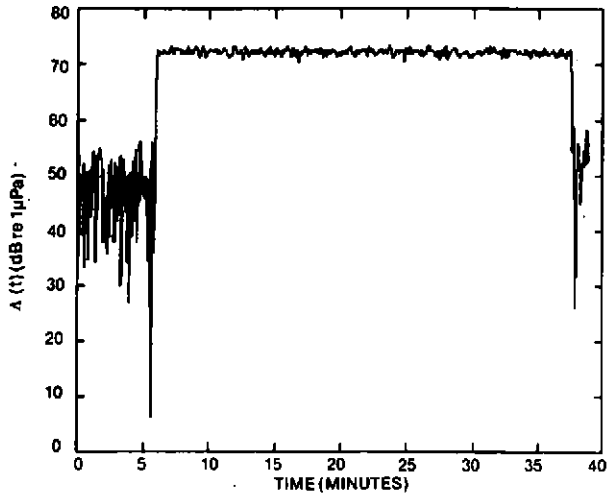

Fig. 2. The level in dB's re 1 μPa of the square of the amplitude of a 30 Hz tone vs. time. Note the tone was on for approximately 30 min.

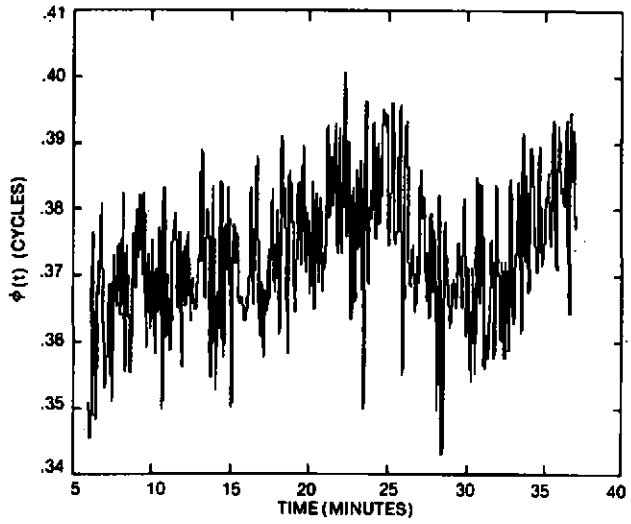

Fig. 3. The phase of the 30 Hz tone.

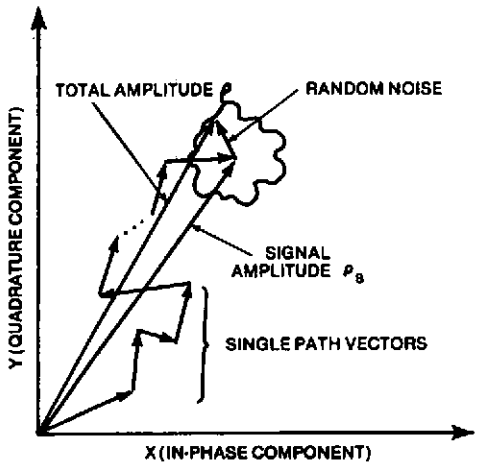

Fig. 4. Polar representation of a received narrowband filtered, demodulated CW tone.

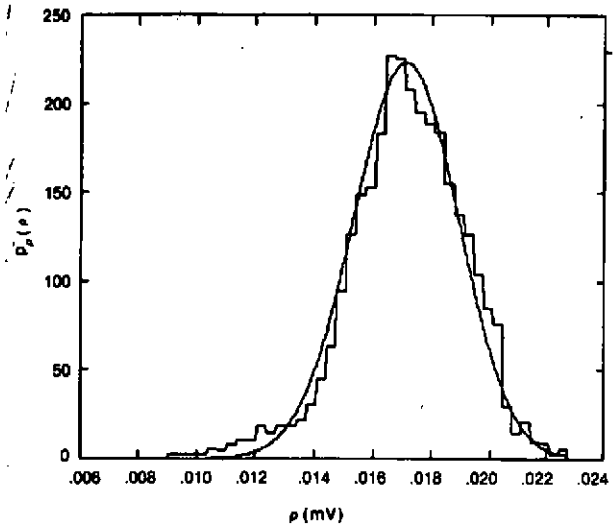

Fig. 5. Histogram of the envelope amplitude and the Rician pdf, Equ (3).

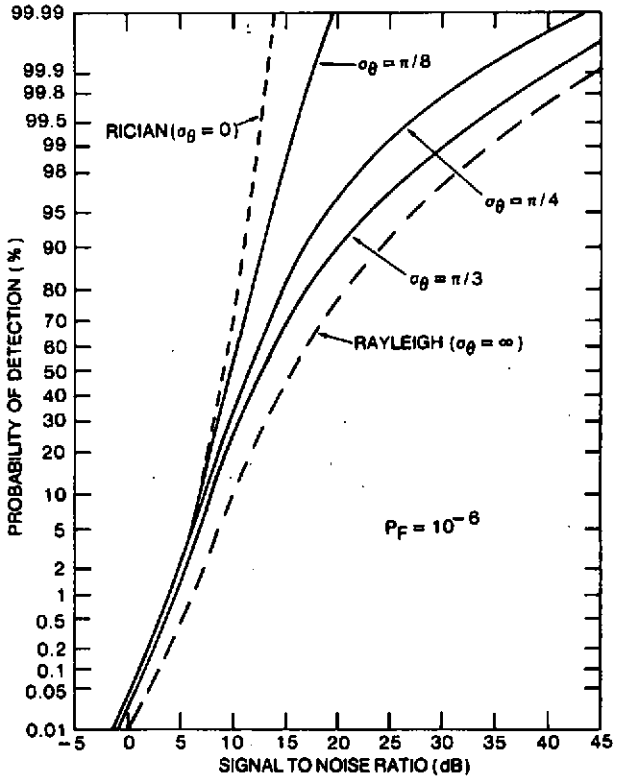

Fig. 6. The detection curves for a narrowband tone in the unsaturated, partially saturated, and fully saturated regimes.